# SUPPLEMENTARY MATERIAL

# Analysis of unstable modes distinguishes mathematical models of flagellar motion

PV Bayly and KS Wilson

**SUPPLEMENTARY MATERIAL**

**A. METHODS: Solution of eigenvalue problems by the method of weighted residuals**

Stability analyses of the linearized equations of motion and boundary conditions were performed by the method of weighted residuals [31] with up to $N = 16$ trial functions to obtain a matrix form of the eigenvalue problem. In each of the cases considered here the equation for the eigenfunctions (mode shapes) can be written as

$$\tilde{\psi}'''' - \mathcal{L}''[\tilde{\psi}] + \bar{\sigma}\tilde{\psi} = 0, \tag{A.1}$$

where $\mathcal{L}''[\tilde{\psi}] = \frac{d^2}{d\bar{s}^2}\mathcal{L}[\tilde{\psi}]$, and $\mathcal{L}$ is a linear operator. We can approximate $\tilde{\psi}$ by a linear combination of admissible trial functions [31], thus:

$$\tilde{\psi}(\bar{s}) \approx \sum_{j=1}^{N} q_j Q_j(\bar{s}), \qquad \mathcal{L}''[\tilde{\psi}] \approx \sum_{j=1}^{N} q_j \mathcal{L}''[Q_j] \tag{A.2}$$

This expression is substituted into the eigenfunction equation, and the residual error weighted by each of a set of test functions, $\phi_i(\bar{s})$, is set to zero.

$$\sum_{j=1}^{N} q_j \left\{ \int_0^1 \phi_i \, Q_j''''\, d\bar{s} - \int_0^1 \phi_i \mathcal{L}''[Q_j] d\bar{s} \; + \; \bar{\sigma} \int_0^1 \phi_i Q_j d\bar{s} \right\} = 0, \;\; i = 1, 2, 3, \ldots, N \tag{A.3}$$

Each of the $N$ equations for the weighted residual error may be integrated by parts to obtain

$$\sum_{j=1}^{N} q_j \left\{ \int_0^1 \phi_i'' \, Q_j'' d\bar{s} + \int_0^1 \phi_i' \mathcal{L}'[Q_j] d\bar{s} \; + \; \bar{\sigma} \int_0^1 \phi_i Q_j d\bar{s} \right\}$$

$$+ \sum_{j=1}^{N} q_j \left\{ \left( \phi_i \{ Q_j''' + \mathcal{L}'[Q_j] \} \right) \Big|_0^1 - \left( \phi_i' Q_j'' \right) \Big|_0^1 \right\} = 0, \qquad i = 1, 2, 3, \ldots, N \tag{A.4}$$

This set of equations can be rewritten simply as

$$[K + \; \bar{\sigma} C]\boldsymbol{q} = \mathbf{0}, \tag{A.5}$$

Where the $N \times N$ matrices $K$ and $C$ contain the coefficients of $q_j$ in the $i^{th}$ equation above:

$$C_{ij} = \int_0^1 \phi_i Q_j d\bar{s} \tag{A.6}$$

$$K_{ij} = \int_0^1 \phi_i'' \, Q_j'' d\bar{s} + \int_0^1 \phi_i' \mathcal{L}'[Q_j] d\bar{s} + \left( \phi_i \{ Q_j''' + \mathcal{L}'[Q_j] \} \right) \Big|_0^1 - \left( \phi_i' Q_j'' \right) \Big|_0^1 . \tag{A.7}$$

Note that $K$ may, in general, depend on $\bar{\sigma}$. The matrix elements were calculated numerically and the resulting matrix eigenvalue problem was solved using MATLAB software (The Mathworks, Natick, MA). The free vibration modes of a uniform, fixed-free beam were used as trial functions ($Q_j$) for flagella with fixed-free boundary conditions, and the modes of a uniform free-free bar were used as trial functions for the swimming flagellum.

The approach above is general, and Eqs. A.5-A.7 may be applied to each model with the only difference being in the specific form of the linear operator associated with the shear force.

For the sliding-controlled model: $\mathcal{L}''[\tilde{\psi}] = \bar{\chi}\tilde{\psi}''$. (A.8)

For the curvature-controlled model: $\mathcal{L}''[\tilde{\psi}] = \frac{\bar{\delta}}{1+\bar{\eta}\bar{\sigma}}\tilde{\psi}'''$. (A.9)

For the geometric clutch model: $\mathcal{L}''[\tilde{\psi}] = [\bar{c}_1(\sigma)(1-\bar{s})\tilde{\psi}']'' + \bar{c}_2(\sigma)\tilde{\psi}''$. (A.10)

For example, the components of the stiffness matrix for the geometric clutch model are:

$$K_{ij}^{(1)} = \int_0^1 \phi_i'' \, Q_j'' d\bar{s} \quad \text{(A.11a)}$$

$$K_{ij}^{(2)} = \int_0^1 \phi_i' \left( [\bar{c}_1(\sigma)(1-\bar{s})Q_j']' + \bar{c}_2(\sigma)Q_j' \right) d\bar{s} \quad \text{(A.11b)}$$

$$K_{ij}^{(3)} = \left( \phi_i Q_j''' - \phi_i' Q_j'' \right)\Big|_0^1 \quad \text{(A.11c)}$$

$$K_{ij}^{(4)} = \phi_i \left( [\bar{c}_1(\sigma)(1-\bar{s})Q_j']' + \bar{c}_2(\sigma)Q_j' \right)\Big|_0^1 \quad \text{(A.11d)}$$

$$K = K^{(1)} + K^{(2)} + K^{(3)} + K^{(4)} \quad \text{(A.12)}$$

The matrix $K$ is then used with the matrix $C$ (from Eq. A.6) in the matrix eigenvalue problem (Eq. A.5). Analogous matrices may be constructed for the sliding-controlled and curvature-controlled models. The matrix $C$ is the same for each model.

The following trial and test functions were used for each eigenanalysis, based on the free vibration modes of the uniform, fixed-free, Euler-Bernouilli beam:

$$Q_i(\bar{s}) = a_i(\cos b_i\bar{s} - \cosh b_i\bar{s}) + (\sin b_i\bar{s} + \sinh b_i\bar{s}) \quad \text{(A.13)}$$

$$\phi_i(\bar{s}) = a_i(-\cos b_i\bar{s} - \cosh b_i\bar{s}) + (-\sin b_i\bar{s} + \sinh b_i\bar{s}) \quad \text{(A.14)}$$

where the coefficients are:

$$b_i = 1.875, 4.694, 7.855, 10.996, 14.137, \ldots, \frac{(2i-1)\pi}{2} \ (i > 5), \ldots \quad \text{(A.15)}$$

$$a_i = (-\sin b_i + \sinh b_i)/(\cos b_i + \cosh b_i) \quad \text{(A.16)}$$

**B. EXAMPLES: STABILITY ANALYSIS OF AXIALLY-LOADED EULER-BERNOUILLI BEAMS**

The stability analysis procedures are demonstrated by applying them to identify and characterize the buckling and flutter modes of an axially loaded beam. In the first case the direction of the load $P$ (positive in compression) is held constant (horizontal as shown in inset to **Fig. S1a**). In the second case the load remains tangent to the beam (a "follower" load; see inset to **Fig. S3a**). The inertia of the beam (mass per unit length $\rho A$) is included; it is embedded in a viscous fluid which provides a transverse resistive force $f_N = -c_N v_N$.

The linearized equation for small-amplitude motion in both cases is [1]

$$EI\psi_{,ssss} + \mathrm{P}\psi_{,ss} + c_N\psi_{,t} + \rho A\psi_{,tt} = 0 \tag{B.1}$$

After substitution of the assumed solution $\psi(s,t) = \exp(\sigma t)\,\tilde{\psi}\,(s)$ the non-dimensional equation for the mode shapes is:

$$\tilde{\psi}'''' + \overline{\mathrm{P}}\tilde{\psi}'' + (\bar{\sigma} + \gamma\bar{\sigma}^2)\tilde{\psi} = 0, \tag{B.2}$$

where $\bar{\sigma} = \sigma c_N L^4/EI$ as before, $\bar{P} = PL^2/EI$, and $\gamma = \rho AEI/c_N^2 L^4$.

For the constant horizontal load the boundary conditions are

| | | |
|---|---|---|
| (S.2) (i) | Zero angle at base: | $\tilde{\psi}(0) = 0$ |
| (S.2) (ii) | Zero normal motion at base: | $\tilde{\psi}'''(0) + \bar{P}\tilde{\psi}'(0) = 0$ |
| (S.2) (iii) | Zero bending moment at distal end: | $\tilde{\psi}'(1) = 0$ |
| (S.2) (iv) | (Horizontal) Transverse force balance at distal end: | $\tilde{\psi}''(1) + \bar{P}\tilde{\psi}(1) = 0$ |

For the follower (tangent) load, at the distal end the boundary condition becomes

| | | |
|---|---|---|
| (S.2) (i) | (Follower) Zero transverse force at distal end: | $\tilde{\psi}''(1) = 0$ |

The characteristic polynomial is

$$\beta^4 + \overline{\mathrm{P}}\beta^2 + (\bar{\sigma} + \gamma\bar{\sigma}^2) = 0. \tag{B.3}$$

For the constant load the eigenvalue problem is:

$$\begin{bmatrix} \cdots & 1 & \cdots \\ \cdots & \beta_n^3 + \overline{\mathrm{P}}\beta_n & \cdots \\ \cdots & \beta_n e^{\beta_n} & \cdots \\ \cdots & \beta_n^2 e^{\beta_n} + \overline{\mathrm{P}} e^{\beta_n} & \cdots \end{bmatrix} \begin{Bmatrix} A_1 \\ A_2 \\ A_3 \\ A_4 \end{Bmatrix} = \begin{Bmatrix} 0 \\ 0 \\ 0 \\ 0 \end{Bmatrix}, \quad \text{n=1, 2, 3, 4} \tag{B.4}$$

For the follower load the eigenvalue problem is:

$$\begin{bmatrix} \cdots & 1 & \cdots \\ \cdots & \beta_n^3 + \overline{\mathrm{P}}\beta_n & \cdots \\ \cdots & \beta_n e^{\beta_n} & \cdots \\ \cdots & \beta_n^2 e^{\beta_n} & \cdots \end{bmatrix} \begin{Bmatrix} A_1 \\ A_2 \\ A_3 \\ A_4 \end{Bmatrix} = \begin{Bmatrix} 0 \\ 0 \\ 0 \\ 0 \end{Bmatrix}, \quad \text{n=1, 2, 3, 4} \tag{B.5}$$

For both cases, when $\bar{\sigma}$ is a valid eigenvalue the determinant, $D(\bar{\sigma})$, of the matrix on the left hand side vanishes.

*Case 1 - Buckling under constant-direction horizontal load*

Initially, the modes of the beam's response are decaying oscillations; the non-dimensional eigenvalue (characteristic exponent $\bar{\sigma} = \bar{\alpha} + i\bar{\omega}$) have small negative real parts ($\bar{\alpha} < 0$) and non-zero imaginary parts ($\bar{\omega} \neq 0$) corresponding to damped natural frequencies of transverse vibration of the beam. As the horizontal load increases, the magnitudes of $\bar{\omega}$ decrease, until at a critical load of $\bar{P} = \pi^2/4$ two eigenvalues converge on the real axis and one crosses into the right half-plane (**Fig. S1a-b**). At $\bar{P} = 3$, the locations of the eigenvalues are shown as minima of the determinant $D(\bar{\sigma})$ (**Fig. S1c**). For each of the three lowest-frequency modes, the corresponding mode shape (eigenfunction) is shown in **Fig. S2**. The eigenvalue $\bar{\sigma}$ of the first mode has zero imaginary part ($\bar{\omega} = 0$) and positive real part, ($\bar{\alpha} > 0$), which are the hallmarks of static instability. In physical beams, and beam models that include nonlinear stiffening terms, this instability leads to a pitchfork bifurcation.

*Case 2 -Flutter due to follower load*

As the follower load increases, pairs of eigenvalues collide and split, with one eigenvalue from each collision crossing into the right half-plane with non-zero imaginary part ($\bar{\omega} \neq 0$, **Fig. S3a-b**). This dynamic instability ("flutter") arises as predicted by Plaut and Infante [2]; in fully nonlinear beam models it leads to a Hopf bifurcation and limit cycle behavior above the critical load. The locations of the eigenvalues at a load of $\bar{P} = 130$ are seen as minima of $D(\bar{\sigma})$ (**Fig. S3c**). The mode shapes corresponding to the three least stable eigenvalue are shown in **Fig. S4**.

For both the constant-direction and follower load, the current approach identifies well-known buckling and flutter instabilities at the correct parameter values [1, 2]. Notably, for a given set of parameters, multiple modes are found that satisfy the equation of motion. In these cases, even if one mode is periodic or decaying, an unstable mode will dominate the response.

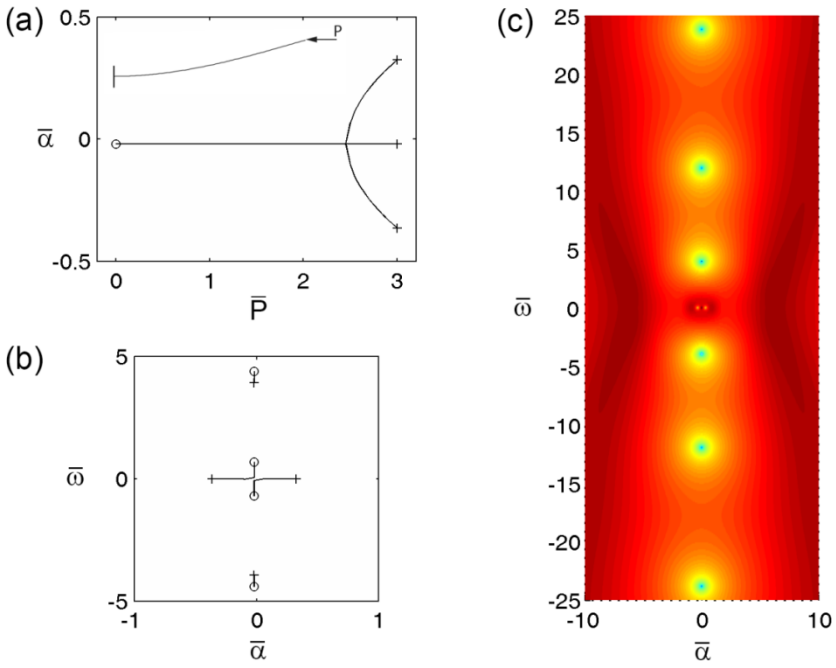


**Figure S1.** Buckling instability of the beam with horizontal tip load (inset). (a) Real part $\bar{\alpha}$ of eigenvalue (characteristic exponent $\bar{\sigma}$) vs non-dimensional load $\bar{P}$. (b) Path of eigenvalues in the complex plane for $0 < \bar{P} < 3$ (o: start; +: end). (c) Image of $\ln|D(\bar{\sigma})|$ as a function of $\bar{\sigma} = \bar{\alpha} + i\bar{\omega}$. Eigenvalues are found at local minima (blue) of the magnitude of the determinant, $|D(\bar{\sigma})|$. Unstable modes have $\bar{\alpha} > 0$. Note that the two local minima close to the origin, corresponding to real eigenvalues in panel (b), exist but are barely perceptible.

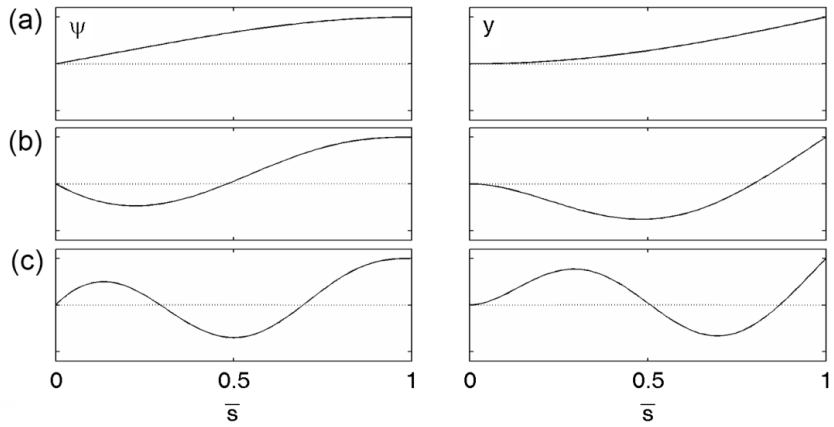


**Figure S2.** First three (lowest-frequency) mode shapes of the Euler-Bernouilli beam with horizontal tip load $\bar{P} = 3$. Mode shapes are shown in terms of angle $\psi(\bar{s})$ on the left and transverse displacement $y(\bar{s})$ on the right. Non-dimensional eigenvalue for each mode are $\bar{\sigma} = \bar{\alpha} + i\bar{\omega}$ with: (a) $\bar{\alpha} = 0.325$; $\bar{\omega} = 0$ (unstable). (b) $\bar{\alpha} = -0.02$; $\bar{\omega} = 3.94$ (stable). (c) $\bar{\alpha} = -0.02$; $\bar{\omega} = 11.96$ (stable). The first mode is statically unstable (buckling mode: $\bar{\alpha} > 0$, $\bar{\omega} = 0$); the remaining modes are oscillatory but stable. Each panel contains two curves: solid line: real part of the mode shape; dashed line: imaginary part.

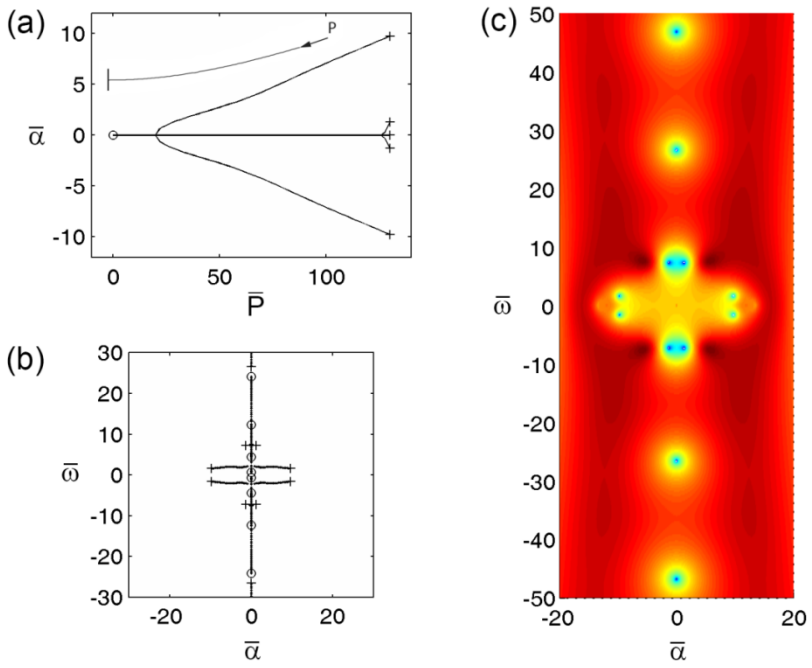


**Figure S3.** Flutter instability of the beam with follower tip load (inset). (a) Real part $\bar{\alpha}$ of eigenvalue vs non-dimensional load $\bar{P}$. (b) Path of eigenvalues in the complex plane for $0 < \bar{P} < 130$ (o: start; +: end). (c) Image of $\ln|D(\bar{\sigma})|$ as a function of $\bar{\sigma} = \bar{\alpha} + i\bar{\omega}$. Eigenvalues are found at local minima (blue) of the magnitude of the determinant, $|D(\bar{\sigma})|$. Unstable modes have $\bar{\alpha} > 0$.

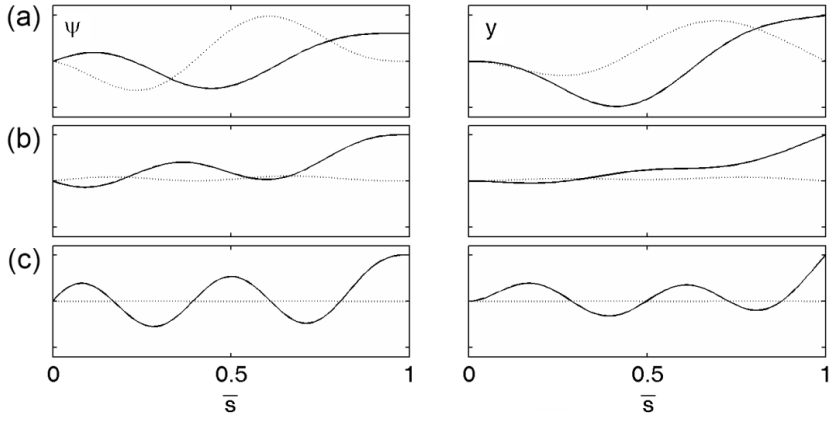


**Figure S4.** First three mode shapes of the Euler-Bernouilli beam with follower tip load $\bar{P} = 130$. Mode shapes are shown in terms of angle $\psi(\bar{s})$ on the left and transverse displacement $y(\bar{s})$ on the right. Non-dimensional eigenvalues for each mode are $\bar{\sigma} = \bar{\alpha} + i\bar{\omega}$ with: (a) $\bar{\alpha} = 9.73$; $\bar{\omega} = 1.60$ (unstable). (b) $\bar{\alpha} = 1.27$; $\bar{\omega} = 7.29$ (unstable). (c) $\bar{\alpha} = -0.02$; $\bar{\omega} = 26.58$ (stable). The first two modes are dynamically unstable (flutter modes: $\bar{\alpha} > 0$, $\bar{\omega} \neq 0$); the remaining modes are oscillatory but stable. Solid line: real part of the mode shape; dashed line: imaginary part.

## C. SENSITIVITY OF EIGENVALUES OF FLAGELLAR MODELS TO PARAMETERS

The sensitivity of flagella behavior to model parameters can be determined from the changes in eigenvalues as the parameter is varied. **Figure S5** shows the effects of flagellar length, $L$, flexural rigidity, $EI$, and resistive force coefficient, $c_N$. The real part of each eigenvalue describes relative stability (the rate of exponential growth or decay) and the imaginary part describes the frequency of oscillations.

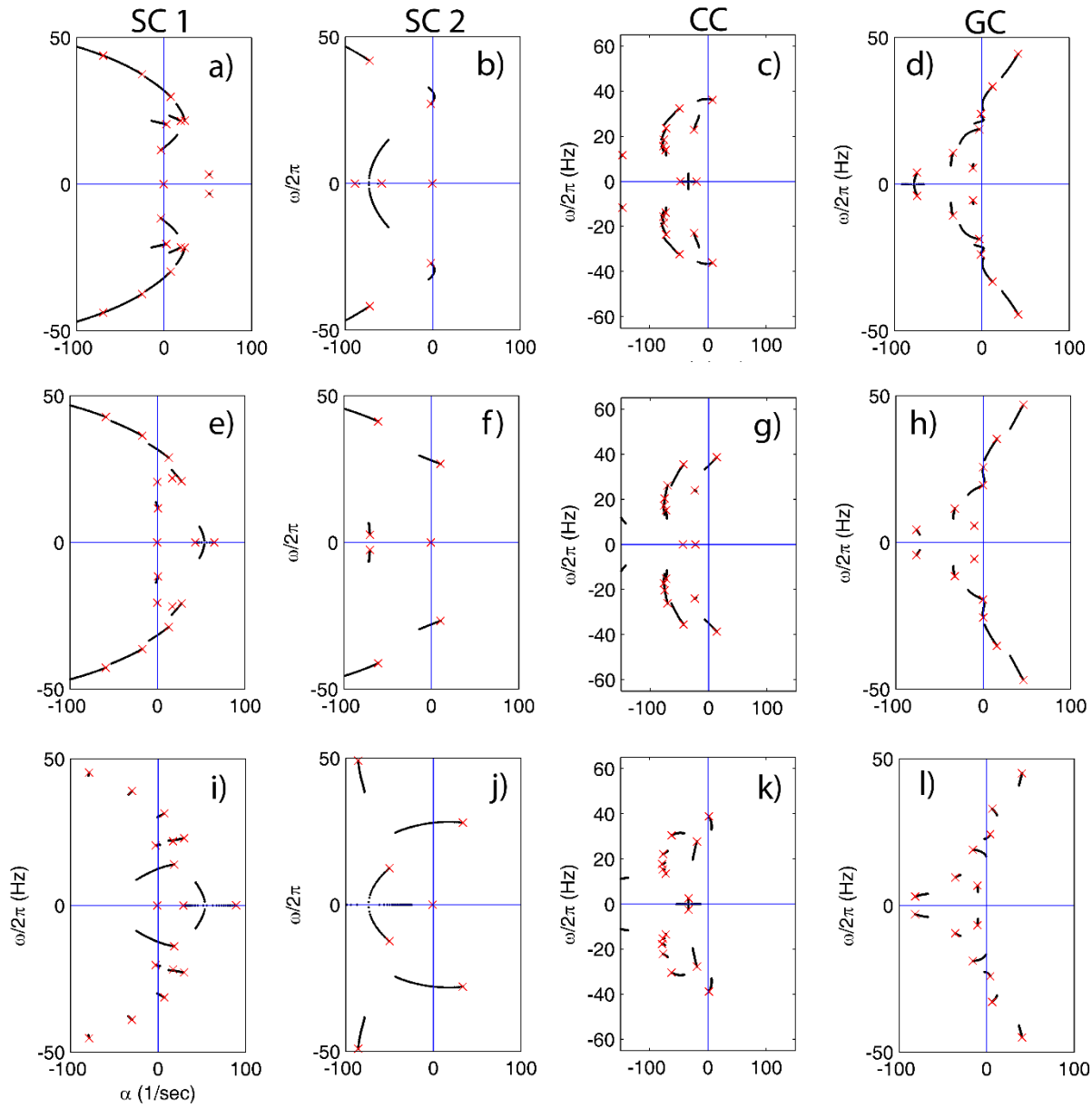


**Figure S5**. Eigenvalue paths as physical parameters are varied. (Column 1, SC1) Sliding-controlled model with sliding at the base; (Column 2, SC 2) Sliding-controlled model with no sliding at the base; (Column 3, CC) Curvature-controlled model; (Column 4, GC) Geometric clutch model. Row 1 (a-d): Eigenvalue paths as length, $L$, is increased from 50 μm to 60 μm. Row 2 (e-h): Eigenvalue paths as flexural rigidity, $EI$, is decreased from 2000 to 1500 pN- μm$^2$. Row 3 (i-l): Eigenvalue paths as resistive force coefficient, $c_N$, is increased from 0.0025 to 0.005 pN-s/ μm$^2$. In each case the red "x" symbol denotes the final eigenvalue.

**D. MOVIES: ANIMATIONS OF UNSTABLE OR NEUTRALLY-STABLE MODES**

**Movie S1**: Periodic mode of sliding-controlled model with sliding at the base (Case 1): $\alpha$=0, $\omega/2\pi$=20.6 Hz.

**Movie S2**: Unstable mode of sliding-controlled model with sliding at the base (Case 1): $\alpha$=51.3/s, $\omega/2\pi$=3.3 Hz.

**Movie S3**: Periodic mode of sliding-controlled model with no sliding at the base (Case 2): $\alpha$=0, $\omega/2\pi$=28 Hz.

**Movie S4**: Oscillatory unstable mode of curvature-controlled model: $\alpha$=5.49/s, $\omega/2\pi$=36.3 Hz.

**Movie S5**: Oscillatory unstable mode of geometric clutch model: $\alpha$=38.5/s, $\omega/2\pi$=43.2 Hz.

**REFERENCES - SUPPLEMENT**

[1] L. N. Virgin, *Vibration of Axially-Loaded Structures*. New York: Cambridge University Press, 2007.
[2] R. H. Plaut and E. F. Infante, "The effect of external damping on the stability of Beck's column," *International Journal of Solids and Structures,* vol. 6, pp. 491-496, 1970.